

Charged excitons in two-dimensional transition-metal dichalcogenides – semiclassical calculation of Berry-curvature effects

A. Hichri* and S. Jaziri†

*Laboratoire de Physique des Matriaux, Faculté des Sciences de Bizerte,
Université de Carthage, 7021 Zarzouna, Tunisie and
Laboratoire de Physique de la Matière Condensée, Faculté des Sciences de Tunis,
Université de Tunis El Manar, 2092 El Manar, Tunisie*

M. O. Goerbig

*Laboratoire de Physique des Solides, CNRS UMR 8502,
Université Paris-Sud, Université Paris Saclay, 91405 Orsay Cedex, France*
(Dated: July 31, 2018)

We theoretically study the role of the Berry curvature on neutral and charged excitons in two-dimensional transition-metal dichalcogenides. The Berry curvature arises due to a strong coupling between the conduction and valence bands in these materials that can to great extent be described within the model of massive Dirac fermions. The Berry curvature lifts the degeneracy of exciton states with opposite angular momentum. Using an electronic interaction that accounts for non-local screening effects, we find a Berry-curvature induced splitting of ~ 17 meV between the $2p_-$ and $2p_+$ exciton states in WS_2 , consistent with experimental findings. Furthermore, we calculate the trion binding energies in WS_2 and WSe_2 for a large variety of screening lengths and different dielectric constants for the environment. Our approach indicates the prominent role played by the Berry curvature along with non-local electronic interactions in the understanding of the energy spectra of neutral and charged excitons in transition-metal dichalcogenides and in the interpretation of their optical properties.

I. INTRODUCTION

Monolayer transition-metal dichalcogenides (TMDC) are a particular class of two-dimensional (2D) materials that exhibit massive Dirac fermions at the two inequivalent valleys K and K' in the first Brillouin zone [1–12]. Beyond graphene, they are therefore a fascinating condensed-matter platform for studying relativistic quantum mechanics in low spatial dimensions. A prominent physical phenomenon, where these relativistic effects are expected to occur, is the formation of excitons. Indeed, in several undoped 2D TMDC, such as MoS_2 , MoSe_2 , WS_2 , or WSe_2 , the Fermi level is situated in the direct band gap, and an electron promoted to the conduction band is strongly bound to the hole left behind in the valence band to form a neutral exciton. Very soon, relatively strong exciton binding energies were found experimentally [13–16].

Contrary to excitons in many 2D and 3D materials, the experimentally obtained spectrum could only be poorly fitted by the 2D hydrogen model [13, 17]. A possible source for this discrepancy was identified in the form of a particular non-local interaction potential due to complex screening effects in the layered material [9, 11, 18, 19]. While such screening effects are likely to play a role in the quantitative understanding of the exciton spectra, a

qualitatively new perspective was proposed by Zhou *et al.* [20] and Srivastava and Imamoglu [21] who point out prominent band coupling effects. Even if the electron resides in the conduction and the hole in the valence band, the bands are two faces of the same medal, e.g. within a description of a massive Dirac model – the projection to a single band is then accompanied by additional Berry-curvature terms. These terms consist of a momentum that is coupled to local electric fields generated by the Coulomb interaction between the electron and the hole. They yield corrections to the exciton spectrum that are on the order of a α^2 , where the coupling constant $\alpha = \sqrt{\Omega}/a_B$ is the ratio between the Berry curvature $\Omega = \hbar^2/\Delta\mu$ at the direct gap Δ (μ is the reduced exciton mass) and the effective Bohr radius $a_B = \hbar^2\kappa/\mu e^2$, in terms of the dielectric constant κ of the environment [22]. While these corrections are negligible in large-gap systems, since $\alpha \propto 1/\sqrt{\Delta}$, they are expected to be pertinent in 2D TMDC, where $\alpha \sim 1$, namely in the ns excitonic states due to their strong decrease with distance [22].

In the present paper, we discuss these band-coupling effects on charged excitons (trions). These trions are formed when the semiconducting material is slightly doped, in which case electron-electron interactions favor bound states between the additional charges and neutral excitons. Similarly to neutral excitons that are also briefly revisited here, we show that the Berry-curvature corrections yield a lower binding energy as compared to the case where they are neglected. As for neutral excitons, this is due to the short-range repulsive character of the terms including the Berry curvature. Our calcu-

* Also at Laboratoire de Physique des Matriaux, Faculté des Sciences de Bizerte, Université de Carthage, 7021 Zarzouna, Tunisie.

† Sihem.Jaziri@fsb.rnu.tn

lations are performed for interaction potentials that include non-local screening effects in order to allow for a quantitative comparison with numerical and experimental data.

The paper is organized as follows. In Sec. II, we revisit neutral excitons, starting from a quantum-mechanical approach to include Berry-curvature corrections at linear order in the one-particle Hamiltonian (Sec. II A) and the exciton Hamiltonian (Sec. II B). Section III is then devoted to a generalization of the approach to charged excitons (trions). The formal aspects are presented in Sec. III A for the semiclassical Berry-curvature term and in Sec. III B for the Darwin term, while Sec. III C is devoted to a quantitative study of the trion binding energies.

II. QUANTUM HAMILTONIAN OF NEUTRAL EXCITONS IN THE PRESENCE OF BAND COUPLING

In the present section, we review the theoretical approach proposed by Zhou *et al.* [20] and Srivastava and Imamoglu [21] to take into account corrective terms in the excitonic Hamiltonian that arise due to a non-zero Berry-curvature. It serves us also for the generalization of these terms to trions in Sec. III.

A. Single-particle considerations

Let us consider the Hamiltonian of a Bloch electron restricted to a single band α

$$H = H_\alpha(\mathbf{k}) + V(\mathbf{r}), \quad (1)$$

where $H_\alpha(\mathbf{k})$ is simply the energy of the band we are interested in (be it an electron or a hole band), as a function of the wave vector \mathbf{k} , and $V(\mathbf{r})$ is an external potential that varies smoothly on the lattice scale. Notice that this description is problematic in the sense that the position operator \mathbf{r} necessarily mixes states of other bands that we want to discard in the low-energy model. In this sense \mathbf{k} and \mathbf{r} are not canonical quantum variables but rather (gauge-invariant) semi-classical variables or averaged quantities projected to a single band α . This leads to the semiclassical equations of motion for Bloch electrons and the introduction of the Berry curvature, which modifies the electron's velocity [23].

Instead of using the above-mentioned semiclassical equations of motion, we try to construct here a quantum Hamiltonian that yields, to lowest order in the magnetic field and the Berry curvature, the same equations of motion. Since the Berry curvature plays the role of a magnetic field in reciprocal space, we introduce the gauge-invariant momentum and position operators

$$\mathbf{p} \rightarrow \mathbf{\Pi} = \mathbf{p} + \frac{e}{2} \mathbf{B} \times \mathbf{r} \quad \mathbf{r} \rightarrow \mathbf{R} = \mathbf{r} + \frac{1}{2\hbar} \Omega_\alpha \times \mathbf{p}, \quad (2)$$

in a Peierls-type approach, where B is the magnetic field and Ω_α the Berry curvature of the band α directed in the direction perpendicular to the 2D plane and $-e$ is the charge of an electron. With the help of the usual commutation relations $[x_j, p_{j'}] = i\hbar\delta_{j,j'}$ for the canonical variables \mathbf{r} and \mathbf{p} , one obtains

$$[\Pi_x, \Pi_y] = -ie\hbar B \quad [X, Y] = i\Omega_\alpha, \quad (3)$$

in agreement with the semiclassical equations of motion. The quantum Hamiltonian is thus obtained from Eq. (1) with the help of the substitution (2),

$$\hat{H} = \hat{H}_0 \left(\frac{\mathbf{p} + e\mathbf{B} \times \mathbf{r}/2}{\hbar} \right) + \hat{V} \left(\mathbf{r} + \frac{1}{2\hbar} \Omega_\alpha \times \mathbf{p} \right). \quad (4)$$

To justify the consistency of this quantum Hamiltonian, we retrieve the semiclassical equations of motion from the Heisenberg equations of motion

$$i\hbar\dot{X}_\mu = [X_\mu, \hat{H}] \quad i\hbar\dot{\Pi}_\mu = [\Pi_\mu, \hat{H}] \quad (5)$$

and the commutator

$$\begin{aligned} [X_\mu, \Pi_{\mu'}] &= [x_\mu + \epsilon_{\mu\nu\sigma}(\Omega_\alpha)_\nu p_\sigma/2\hbar, p_{\mu'} + e\epsilon_{\mu'\nu'\sigma'} B_{\nu'} x_{\sigma'}/2] \\ &\simeq i\delta_{\mu,\mu'}(\hbar + e\Omega_\alpha B) = i\hbar\delta_{\mu,\nu}, \end{aligned} \quad (6)$$

to lowest order in the B and Ω_α . In the last line we have introduced a ‘‘deformed’’ Planck constant $\tilde{\hbar} = \hbar + eB\Omega_\alpha$ – this is due to a modified density of states, but arises only at second order (product of $B\Omega_\alpha$). Since we are interested, here, only in corrections at order one (and in addition in the $B = 0$ case), we will set $\tilde{\hbar} = \hbar$ at the end. With this help, one finds from the Heisenberg equations of motion

$$\begin{aligned} \dot{\mathbf{R}} &= \left(1 + \frac{eB\Omega_\alpha}{\hbar} \right) \frac{\partial \hat{H}_0}{\partial \mathbf{\Pi}} + \frac{\partial \hat{V}}{\hbar \partial \mathbf{R}} \times \Omega_\alpha \\ \dot{\mathbf{\Pi}} &= - \left(1 + \frac{eB\Omega_\alpha}{\hbar} \right) \frac{\partial \hat{V}}{\partial \mathbf{R}} - e \frac{\partial \hat{H}_0}{\partial \mathbf{\Pi}} \times \mathbf{B}, \end{aligned} \quad (7)$$

which coincide indeed with the semiclassical equations of motion to linear order in B and Ω [24].

To complete the quantum description at this order of the expansion, we also need to expand the Hamiltonian (4) to the same order,

$$\hat{H} = \hat{H}_0(\mathbf{p}) + \hat{V}(\mathbf{r}) + \frac{1}{2\hbar} \frac{\partial \hat{V}}{\partial \mathbf{r}} \cdot (\Omega_\alpha \times \mathbf{p}) + \frac{e}{2\hbar} \frac{\partial \hat{H}_0}{\partial \mathbf{p}} \cdot (\mathbf{B} \times \mathbf{r}), \quad (8)$$

which is now expressed in terms of the canonical variables \mathbf{r} and \mathbf{p} and thus amenable to the usual quantum-mechanical treatment. This result coincides with the Hamiltonian obtained by Zhou *et al.* for $B = 0$ [20].

B. Corrective Berry-curvature terms in the excitonic Hamiltonian

The above discussion has direct consequences for the quantum-mechanical description of excitons in multiband

systems, where the third term in the Hamiltonian (8) arises from the mutual interaction between the electron and the hole constituting the (neutral) exciton. The exciton consists of an electron in the valence band, described by the (band) Hamiltonian in the continuum

$$\hat{H}_0^e = \frac{\Delta}{2} + \frac{\mathbf{p}_1^2}{2m_e} \quad (9)$$

and a hole in the valence band with

$$\hat{H}_0^h = \frac{\Delta}{2} + \frac{\mathbf{p}_2^2}{2m_h}, \quad (10)$$

where m_e and m_h are the band masses for the electron and the hole, respectively, and Δ is the direct gap between the valence and the conduction band. The momenta \mathbf{p}_1 and \mathbf{p}_2 are measured from the reciprocal-space position of the conduction-band minimum, which coincides with the valence-band maximum in the present case of a direct-gap semiconductor. We consider, here, intra-valley excitons, i.e. where both the electron and the hole reside in the same valley. The electron and the hole interact via an attractive interaction potential $\hat{V}(|\mathbf{r}_1 - \mathbf{r}_2|)$ that we consider as isotropic – one may think of the usual Coulomb interaction with possible corrections due to screening. In most approaches, one simply considers the Hamiltonian $\hat{H}_0^e + \hat{H}_0^h + \hat{V}$, which constitutes the (2D) hydrogen problem in the case of a pure Coulomb interaction. However, the interaction induces corrective terms via the Berry curvature,

$$\hat{H}_B = \frac{1}{2\hbar} \frac{\partial \hat{V}(\rho)}{\partial \boldsymbol{\rho}} \cdot [\Omega_e(\mathbf{p}_1) \times \mathbf{p}_1 + \Omega_h(\mathbf{p}_2) \times \mathbf{p}_2], \quad (11)$$

where $\boldsymbol{\rho} = \mathbf{r}_1 - \mathbf{r}_2$ is the relative coordinate and $\rho = |\boldsymbol{\rho}|$.

One notices from this equation that relative and center-of-mass motion are not decoupled. Indeed, if we use the usual change in coordinates

$$\begin{aligned} M\mathbf{R} &= m_e\mathbf{r}_1 + m_h\mathbf{r}_2, & \boldsymbol{\rho} &= \mathbf{r}_1 - \mathbf{r}_2 \\ \mathbf{P} &= \mathbf{p}_1 + \mathbf{p}_2, & \mathbf{p}/\mu &= \mathbf{p}_1/m_e - \mathbf{p}_2/m_h, \end{aligned} \quad (12)$$

in terms of the total mass $M = m_e + m_h$ and the relative mass $\mu = m_e m_h / M$, the corrective term (11) becomes

$$\begin{aligned} \hat{H}_B &= \frac{1}{2\hbar} \frac{\partial \hat{V}(\rho)}{\partial \boldsymbol{\rho}} \cdot \left[\Omega_e \left(\mathbf{p} + \frac{m_e}{M} \mathbf{P} \right) \times \left(\mathbf{p} + \frac{m_e}{M} \mathbf{P} \right) \right. \\ &\quad \left. - \Omega_e \left(-\mathbf{p} + \frac{m_h}{M} \mathbf{P} \right) \times \left(-\mathbf{p} + \frac{m_h}{M} \mathbf{P} \right) \right], \quad (13) \end{aligned}$$

where we have already used $\Omega_h(\mathbf{q}) = -\Omega_e(\mathbf{q})$, valid for two-band models. This is in line with the case of massive Dirac fermions – a particular case of the two-band models discussed here – because a change in the frame of reference for the center-of-mass motion also affects, due to the associated Lorentz contraction, the relative coordinates. While we consider excitons in the center-of-mass frame of reference (i.e. $\mathbf{P} = 0$), we briefly comment on the case $m_e = m_h$ relevant in 2D transition-metal dichalcogenides

(TMDC). One then finds, to lowest order in Ω_e (i.e. in the absence of gradient terms $\partial\Omega_e/\partial\mathbf{p}$)

$$\hat{H}_B \simeq \frac{1}{2\hbar} \frac{\partial \hat{V}(\rho)}{\partial \boldsymbol{\rho}} \cdot [\Omega(\mathbf{P}/2) \times \mathbf{p}], \quad (14)$$

where $\Omega(\mathbf{p}) = 2\Omega_e(\mathbf{p})$ can be considered as the exciton Berry curvature. Also here one notices the coupling between center-of-mass and relative coordinates. Adding now the Darwin-type term $\Omega(\mathbf{q})\nabla_\rho^2\hat{V}(\rho)/4$, one obtains, in the center-of-mass frame of reference, which we consider from now on, the semiclassical exciton Hamiltonian [20, 22]

$$\begin{aligned} \hat{H}_X &= \frac{\mathbf{P}}{2\mu} + \hat{V}(\rho) \\ &\quad + \frac{1}{2\hbar} \frac{\partial \hat{V}(\rho)}{\partial \boldsymbol{\rho}} \cdot [\Omega(\mathbf{p}) \times \mathbf{p}] + \frac{1}{4} |\Omega(\mathbf{q})| \nabla_\rho^2 \hat{V}(\rho), \end{aligned} \quad (15)$$

in terms of the exciton Berry curvature [25, 26]

$$\Omega(\mathbf{p}) = \Omega_e(\mathbf{p}) + \Omega_e(-\mathbf{p}) \simeq 2\Omega_e(0) \simeq \frac{\hbar^2}{\mu\Delta} \mathbf{e}_z, \quad (16)$$

where \mathbf{e}_z is the unit vector in the z -direction. Notice that Hamiltonian (15) describes the binding energy of the exciton, i.e. we have omitted the gap energy Δ , which appears in the energy to create a free electron and a free hole. From the exciton Hamiltonian (15), one can already draw some conclusions. Most importantly, the last two terms, which depend on the Berry curvature, modify the exciton spectrum as compared to the usual 2D hydrogen model. The latter is retrieved in the limit of large gaps for which the Berry-curvature terms vanish as $\Omega \sim 1/\Delta$, i.e. when the gap becomes by far the largest energy scale. Furthermore, these corrective terms do not play a role in direct-gap semiconductors, where the gap is situated at a time-reversal-invariant momentum, in which case the Berry curvature vanishes. Finally, the Berry-curvature terms play a minor role in states with large angular momentum where the average distance between the electron and the hole increases. This can easily be seen for a $1/r$ -Coulomb-type potential where the last two terms of (15) scale as $1/r^3$, while the direct Coulomb term scales as $1/r$ and the centrifugal terms in the usual manner as $1/r^2$ [22, 27]. Notice also that the chirality of the second last term breaks the rotational symmetry, such that the $m \leftrightarrow -m$ degeneracy is lifted [21].

Notice that, in the above discussion, we have not explicitly taken into account the spin or the valley of the electron and hole constituting the exciton. If we consider 2D TMDC, the strong spin-orbit coupling leads to a locking between spin and valley. This means that, if we consider e.g. spin-up electrons in the K valley (i.e. the highest valence band is occupied by spin-up particles), the spin is reversed when one wants to treat excitons in the K' -valley. The above discussion then remains valid, but we need to change the sign of the Berry curvature, such that the last term in Eq. (15) acquires a minus sign.

C. Revisiting neutral excitons in monolayer WS₂

Before generalizing the above description for neutral excitons to trions, let us first revisit, in view of the Berry-curvature corrections, the exciton binding energy in monolayer WS₂ [28]. We start with some remarks on the pure Coulomb potential $\hat{V}(\rho) = -e^2/\kappa\rho$, which can to large extent be treated analytically. Here, the effective dielectric constant $\kappa = (\varepsilon_{sub} + \varepsilon_{vac})/2$ is the average of the the dielectric permittivity of the substrate, ε_{sub} , and that of the vacuum, ε_{vac} . In the absence of Berry-curvature corrections, one obtains thus the usual 2D hydrogenic spectrum $E_{n,m} = -\text{Ry}/(n + 1/2)^2$, which is degenerate in the angular-momentum quantum number m and only depends on the principal quantum number n . Here, $\text{Ry} \simeq 13 \text{ eV} \times (\mu/m_0)/\kappa^2$ is the effective Rydberg energy for a reduced mass of $\mu = 0.17m_0$ and $\kappa \simeq 1.55$, relevant for WS₂ [13, 22]. The degeneracy in the angular momentum m is lifted due to the chiral Berry-curvature term and splits the level into $\Delta_{n,m} = |E_{n,m+} - E_{n,m-}|$ according to the handedness of the angular momentum [20, 21]. Using the atomic orbital terminology s (for $m = 0$), p_{\pm} (for $m = \pm 1$), d_{\pm} (for $m = \pm 2$) ..., we find $\Delta_{2p} = (64/81)(\Omega/a_B^2)\text{Ry}$, in agreement with Ref. [20] and $\Delta_{3p} = (64/375)(\Omega/a_B^2)\text{Ry}$. The numerical values can be found in the second line of Tab. I, for a value of $a_B = 0.5\text{\AA} \times (m_0/\mu)\kappa \simeq 5 \text{\AA}$ and an upper bound of $\Omega = 10 \text{\AA}^2$ for the Berry curvature [29].

The above numerical values become smaller when non-local screening effects are taken into account, which furthermore lift the degeneracy in the quantum number m already in the absence of Berry-curvature corrections, while keeping the degeneracy in $m \leftrightarrow -m$. The appropriate electron-hole interaction $\hat{V}(\rho)$ is given by the Keldysh potential [30]

$$\begin{aligned} \hat{V}(\rho) &= -\frac{e^2}{\kappa 2\pi} \int \frac{e^{iq\rho} d^2q}{q(1+q\lambda_s)} \\ &= -\frac{\pi e^2}{2\kappa\lambda_s} [H_0(\rho/\lambda_s) - Y_0(\rho/\lambda_s)] \end{aligned} \quad (17)$$

where $H_0(x)$ and $Y_0(x)$ are the Struve and Bessel function of the second kind, respectively, and λ_s , which can be related to the 2D polarizability of the monolayer material, gives a crossover length scale between the long and short range Coulomb interaction. The expressions $\nabla_{\rho}\hat{V}(\rho)$ and $\nabla_{\rho}^2\hat{V}(\rho)$ in the Berry and Darwin terms can be directly calculated and give

$$\begin{aligned} \frac{\partial\hat{V}(\rho)}{\partial\rho} &= -\frac{e^2}{\kappa\lambda_s} \int \frac{dq}{1+q\lambda_s} \frac{\partial J_0(q\rho)}{\partial\rho} = \frac{e^2}{\kappa\lambda_s} \int \frac{q dq}{1+q\lambda_s} J_1(q\rho) \\ \frac{\partial^2\hat{V}(\rho)}{\partial\rho^2} &= \frac{e^2}{\kappa\lambda_s} \int \frac{q dq}{1+q\lambda_s} \left[qJ_0(q\rho) - \frac{J_1(q\rho)}{\rho} \right] \end{aligned} \quad (18)$$

where $J_{\nu}(X)$ are Bessel functions of the first kind. The asymptotic behavior of $\hat{V}(\rho)$ is $\hat{V}(\rho \rightarrow \infty) \sim 1/\rho$ and $V(\rho \rightarrow 0) \sim -\frac{1}{\lambda_s} [\ln(\rho/2\lambda_s) + \gamma]$ where $\gamma \sim 0.5772$ is Eu-

ler's constant. The crossover between these two behaviors is characterized by the length scale λ_s . By the simplest possible matching of the two asymptotic behaviors and to avoid the divergence of the integral of the Bessel function $qJ_{\nu}(q\rho)$, we can construct an approximated expression for $V(\rho)$ in terms of elementary functions [31]

$$\hat{V}(\rho) = \frac{e^2}{\kappa\lambda_s} \left[\ln\left(\frac{\rho}{\rho + \lambda_s}\right) + (\gamma - \ln 2)e^{-\rho/\lambda_s} \right] \quad (19)$$

which gives an accurate description of the screening potential also at intermediate values of (ρ/λ_s) . In this form, the resulting energy of excitonic systems is a function of only λ_s and κ . Now, to determine the new eigenvalues of the Hamiltonian given in Eq. (15), one needs calculate the matrix elements of \hat{H}_X in the basis of 2D hydrogenic eigenfunction, which become the exact ground state wavefunction in the limit of weak screening. The Berry term \hat{H}_B [Eq. (14)], has only off-diagonal matrix elements which are non-zero; it acts on exciton states with opposite angular momentum and thus lifts the degeneracy between $np_+(nd_+)$ and $np_-(nd_-)$ states, This can be seen in the following equation for the Berry-curvature correction

$$\frac{\hat{H}_B}{\text{Ry}} \simeq \frac{ia_B\Omega}{\lambda_s} \left(\frac{1}{\rho} - \frac{1}{\rho + \lambda_s} - \frac{1}{\lambda_s}(\gamma - \ln 2)e^{-\rho/\lambda_s} \right) \frac{1}{\rho} \frac{\partial}{\partial\theta} \quad (20)$$

In contrast to the hydrogenic model with local conventional Coulomb interaction, the energy splitting calculated with the Keldysh potential is substantially smaller, for $\lambda_s = 28\text{\AA}$, $\Delta_{2p} = |E_{2p_+} - E_{2p_-}| = 17 \text{ meV}$ and almost vanishes for $n \geq 4$ (see Tab. I). Consequently, one can consider the Berry curvature correction using Keldysh interaction as just a perturbation, which only introduces a small splitting between the $m \neq 0$ states, in comparison with that using the conventional 2D hydrogenic potential. The obtained $2p$ splitting is consistent with the reported splitting of 10 meV (15 meV) in MoS₂ (WS₂) [32]. The Darwin term is proportional to $\nabla_{\rho}^2\hat{V}$ and leads to an energy shift depending on the quantum number n [20].

In Fig. 1, we plot the calculated first positions of the exciton binding energy $B_{nm} = -E_{nm}$ with various principal and orbital angular momentum quantum numbers, n and m , respectively. Here, E_{nm} are obtained by the diagonalization of the Hamiltonian (15). The large binding energy in monolayer TMDCs results from the enhanced Coulomb interaction due to the strong quantum confinement, reduced dielectric screening and heavy effective masses [9]. This reduction of the exciton binding energy is less pronounced for higher energy exciton states ($B_{2s} < B_{1s}$). We recall that, while the usual $1/\rho$ Coulomb potential gives equal energies $E_{n,m} = E_n$, this $(2n - 1)$ -fold degeneracy is lifted by the screened potential [Eqs. (17) and (19)] which originates from the weak dielectric broadcast in the 2D limit [30]. Our calculations show that the energy of the $m = 1$ ($m = 2$) excited state is lower than that of the $m = 0$ ($m = 1$) excited state

TABLE I. The effect of Berry curvature on the energy splitting of np states.

$\Delta_{n,p}$ (in meV)	$n=2$	$n=3$	$n=4$	$n=5$
with locally-screened interaction	321	69	25	12
with non locally-screened interaction	17	5	1.8	1.6

i.e. $E_{2p} < E_{2s}$ ($E_{3d} < E_{3p}\dots$). The degeneracy between $2s$ and $2p$ states is lifted with $2p_-$ states lying about 37 meV below the $2s$ states. This result is in agreement with other theoretical investigations where $E_{2s} - E_{2p} = 35\text{meV}$ [21, 27, 32, 33].

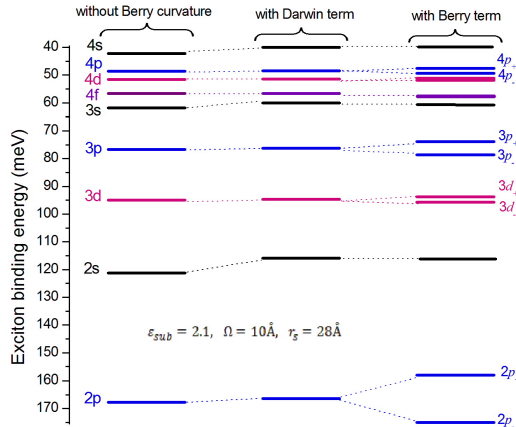


FIG. 1. Theoretical excitonic spectrum reported for WS_2 monolayer deposited on the SiO_2 substrate $\epsilon_{sub} = 2.1$ and exposed to the air $\epsilon_{vac} = 1$ for the screening length $\lambda_s = 28$ Å and $a_B = 5$ Å. The results are obtained by numerical diagonalization of the Hamiltonian given in Eq. (15), using the non-local screening potential and taking into account the Berry curvature correction. We show a mixing and splitting of np and nd states due to the Berry curvature.

Upon the inclusion of the non-local potential and Berry curvature, states with opposite angular momentum mix and split much like in the case of an orbital Zeeman effect. The Darwin term acts mainly on the s -states, due to its very local action [22]. Principally, the energy position of $1s$ exciton state shows a decreasing shift in response to this extra term which, would otherwise remain unaffected by the Berry term. However, the $1s$ ground state $\xi_{1s} = \Delta - B_{1s}$ shifts from 2.079 to 2.101 eV. Consequently, the $1s$ exciton binding energy decreases by 22meV as compared to that obtained in our previous work [28], where the Berry and Darwin terms were neglected. This results in binding energies around 290 meV. For a better comparison with experimental measurements and other theoretical findings, Tab. II summarizes the exciton binding energies in monolayer WS_2 and WSe_2 for a wide range of screening lengths. Varying the screening length and including the Berry correction dramatically changes the results. A general trend appearing

in our calculations is that when the screening length exceeds the Bohr radius the exciton binding energy is weak, while for smaller screening lengths ($\lambda_s \sim a_B$) the exciton becomes more strongly bound. For a suspended WX_2 monolayer, the exciton binding energy reaches 900meV even if the Berry correction is taken into account. On the other hand, the Berry correction decreases significantly with increasing exciton binding energy, i.e. for small λ_s . However, depending on the screening length, the adjustment with Berry correction cannot be made because in a certain range the exciton binding energy differs significantly from the observed value and thus does not agree with experiment. These values can serve as a benchmark for theory.

III. TRION HAMILTONIAN IN THE CONTINUUM LIMIT

In the presence of residual free charge carriers, excitons interact with the surrounding charges and can form charged excitons [39, 40]. The strong Coulomb interaction between the electron and hole leads to a larger trion binding energy. We consider here negatively charged trions that consist of two electrons and one hole all of which reside in the same valley. The approach is easily generalized to positively charged excitons. In this case, we have two electron contributions

$$\hat{H}_0^{ej} = \frac{\Delta}{2} + \frac{\mathbf{p}_{ej}^2}{2m_e} \quad (21)$$

for the electrons e_1 and e_2 , i.e. $j = 1, 2$, in the same band with band mass m_e and a contribution

$$\hat{H}_0^h = \frac{\Delta}{2} + \frac{\mathbf{p}_h^2}{2m_h} \quad (22)$$

from the hole in the valence band. The interaction Hamiltonian contains now three terms

$$\hat{V}(\rho) = \hat{V}(\rho_1) + \hat{V}(\rho_2) - \hat{V}(|\rho_1 - \rho_2|) \quad (23)$$

where $\rho_1 = \mathbf{r}_1 - \mathbf{r}_h$ and $\rho_2 = \mathbf{r}_2 - \mathbf{r}_h$ are the relative coordinates between the two electron positions $\mathbf{r}_1, \mathbf{r}_2$ and the hole position \mathbf{r}_h ,

$$\rho_j = \mathbf{r}_j - \mathbf{r}_h, \quad \rho_1 - \rho_2 = \mathbf{r}_1 - \mathbf{r}_2 \quad (24)$$

TABLE II. Exciton binding energies (given in meV) for both WS₂ and WSe₂ monolayer deposited on SiO₂ substrate. The effective screening radius λ_s varies between ~ 5 and $\sim 25\text{\AA}$. Experimental and theoretical results from literature are collected for comparison. The reduced mass used for WSe₂ monolayer are listed in Ref. [34].

	WS ₂		WSe ₂	
	$\Omega = 0$	$\Omega = 10\text{\AA}^2$	$\Omega = 0$	$\Omega = 10\text{\AA}^2$
$\lambda_s = a_B$	626	480	840	607
$\lambda_s = 1.5a_B$	539	445	724	564
$\lambda_s = 2.5a_B$	439	386	590	493
$\lambda_s = 3.5a_B$	376	341	505	437
$\lambda_s = 4.a_B$	352	322	473	414
$\lambda_s = 5.a_B$	313	290	420	375
Experiment	320 [13] -700 [15, 17]		370 [14], 600 [35]	
Theory	509 [36], 523 [37], 830 [15], 1050 [38]		456 [36], 470 [37], 790 [15]	

Without the Berry-curvature correction, this trion Hamiltonian can be brought into the form

$$\begin{aligned} \hat{H}_T = & \frac{\mathbf{P}^2}{2M_T} + \frac{\mathbf{p}_1^2}{2\mu} + \frac{\mathbf{p}_2^2}{2\mu} + \frac{\mathbf{p}_1 \cdot \mathbf{p}_2}{2m_h} \\ & + \hat{V}(\rho_1) + \hat{V}(\rho_2) - \hat{V}(|\boldsymbol{\rho}_1 - \boldsymbol{\rho}_2|) + \hat{H}_B^T + \hat{H}_D^T \end{aligned} \quad (25)$$

where the term \hat{H}_B^T accounts for the trion Berry-curvature corrections, while \hat{H}_D^T represents a trion Darwin term that arises, in the same manner as for neutral excitons, within relativistic quantum mechanics, but which is beyond the semi-classical description limited to first-order gradient terms in the potential. Again, we have omitted the constant term $3\Delta/2$, which represents the energy to create three non-interacting particles because we are interested in the binding energies, i.e. the negative eigenvalues of the trion Hamiltonian (25).

The Hamiltonian (25) is expressed in terms of the relative coordinates (24) and the trion center-of-mass coordinate $\mathbf{R}_T = [m_e(\mathbf{r}_1 + \mathbf{r}_2) + m_h\mathbf{r}_h]/M_T$, where $M_T = 2m_e + m_h$ is the total mass. The momenta

$$\begin{aligned} \mathbf{P}_T = & \mathbf{p}_{e1} + \mathbf{p}_{e2} + \mathbf{p}_h \\ \mathbf{p}_1 = & \mu \left(\frac{\mathbf{p}_{e1}}{m_e} - \frac{\mathbf{p}_h}{m_h} \right), \quad \mathbf{p}_2 = \mu \left(\frac{\mathbf{p}_{e2}}{m_e} - \frac{\mathbf{p}_h}{m_h} \right) \end{aligned} \quad (26)$$

are conjugate to \mathbf{R} , $\boldsymbol{\rho}_1$ and $\boldsymbol{\rho}_2$, respectively.

A. Berry-curvature correction

Let us now discuss in detail the part \hat{H}_B^T in the Hamiltonian, i.e. take into account the Berry curvature. For one of the trion components, this term arises from the interaction potential generated by the other two components, and the Hamiltonian thus consists of six contribu-

tions,

$$\begin{aligned} \hat{H}_B^T = & \frac{1}{2\hbar} \nabla_{\rho_1} \hat{V} \cdot [\Omega_e(\mathbf{p}_{e1}) \times \mathbf{p}_{e1} + \Omega_h(\mathbf{p}_h) \times \mathbf{p}_h] \\ & + \frac{1}{2\hbar} \nabla_{\rho_1} \hat{V} \cdot [\Omega_e(\mathbf{p}_{e2}) \times \mathbf{p}_{e2} + \Omega_h(\mathbf{p}_h) \times \mathbf{p}_h] \\ & - \frac{1}{2\hbar} \nabla_{\rho_3} \hat{V} \cdot [\Omega_e(\mathbf{p}_{e1}) \times \mathbf{p}_{e1} + \Omega_e(\mathbf{p}_{e2}) \times \mathbf{p}_{e2}], \end{aligned} \quad (27)$$

where we have defined $\boldsymbol{\rho}_3 = \mathbf{r}_1 - \mathbf{r}_2$ as the relative coordinate between the two electrons [41]. Remember that we have opposite Berry curvatures in the different bands, $\Omega_e(\mathbf{k}) = -\Omega_h(\mathbf{k})$, at each wave vector, and we furthermore approximate the Berry curvature by its value at the gap $\Omega_e(\mathbf{k}) \simeq \Omega_e(0)$ [42]. The Berry-curvature contribution thus becomes

$$\begin{aligned} \hat{H}_B^T \simeq & \frac{1}{2\hbar} \nabla_{\rho_1} \hat{V} \cdot [\Omega_e(0) \times (\mathbf{p}_{e1} - \mathbf{p}_h)] \\ & + \frac{1}{2\hbar} \nabla_{\rho_2} V \cdot [\Omega_e(0) \times (\mathbf{p}_{e2} - \mathbf{p}_h)] \\ & - \frac{1}{2\hbar} \nabla_{\rho_3} V \cdot [\Omega_e(0) \times (\mathbf{p}_{e1} + \mathbf{p}_{e2})]. \end{aligned} \quad (28)$$

These expressions turn out to be more complicated than those of the neutral exciton if we aim at expressing them in terms of the momenta (26), and we therefore use immediately two simplifications, valid in the case of 2D TMDC. The first one is to consider conduction and valence bands with the same curvature or band mass, i.e. $m_e = m_h$; and the second approximation consists of a calculation in the center-of-mass frame of the trion, i.e. $\mathbf{P}_T = 0$. We then find

$$\mathbf{p}_{e1} + \mathbf{p}_{e2} = -\mathbf{p}_h \quad (29)$$

and, with $\mu = m_e/2$,

$$\mathbf{p}_h = -\frac{2}{3}(\mathbf{p}_1 + \mathbf{p}_2). \quad (30)$$

We can thus express the Berry-curvature contribution in terms of the excitonic Berry curvature $\Omega(0) = 2\Omega_e(0)$, as

in the case of the neutral exciton, as [43]

$$\begin{aligned} \hat{H}_B^T \simeq & \frac{1}{2\hbar} \nabla_{\rho_1} \hat{V} \cdot [\Omega(0) \times \mathbf{p}_1] + \frac{1}{2\hbar} \nabla_{\rho_2} \hat{V} \cdot [\Omega(0) \times \mathbf{p}_2] \\ & - \frac{1}{2\hbar} \nabla_{\rho_3} \hat{V} \cdot \left[\frac{\Omega(0)}{3} \times (\mathbf{p}_1 + \mathbf{p}_2) \right], \end{aligned} \quad (31)$$

which can be further simplified by getting rid of the redundant variable $\rho_3 = \rho_1 - \rho_2$, such that

$$\begin{aligned} \hat{H}_B \simeq & -\frac{1}{2\hbar} \left(\nabla_{\rho_1} \hat{V} - \frac{1}{3} \nabla_{\rho_1 - \rho_2} \hat{V} \right) \cdot [\Omega(0) \times \mathbf{p}_1] \\ & - \frac{1}{2\hbar} \left(\nabla_{\rho_2} \hat{V} - \frac{1}{3} \nabla_{\rho_2 - \rho_1} \hat{V} \right) \cdot [\Omega(0) \times \mathbf{p}_2], \end{aligned} \quad (32)$$

where the Berry curvature can be expressed explicitly as

$$\Omega(0) = \zeta \frac{\hbar^2}{\mu\Delta} \mathbf{e}_z = 2\zeta \frac{\hbar^2}{m_e\Delta} \mathbf{e}_z = 2\Omega_e(0). \quad (33)$$

The sign $\zeta = \pm$ takes into account whether we consider spin-up particles in the K -valley ($\zeta = +$) or spin-down particles in the K' -valley ($\zeta = -$). Equation (32) is the main result of this section. For the pure Coulomb potential with

$$\hat{V}(\rho) = -\frac{e^2}{\varepsilon\rho}, \quad \nabla_{\rho} \hat{V} = \frac{e^2}{\varepsilon\rho^2} \frac{\rho}{\rho} \quad (34)$$

the Berry-curvature term reads

$$\begin{aligned} \hat{H}_B = & -\zeta \frac{\hbar e^2}{2\mu\varepsilon\Delta} \left[\frac{1}{\rho_1^3} (\mathbf{p}_1 \times \rho_1)_z + \frac{1}{\rho_2^3} (\mathbf{p}_2 \times \rho_2)_z \right] \\ & + \zeta \frac{\hbar e^2}{6\mu\varepsilon\Delta |\rho_1 - \rho_2|^3} [(\mathbf{p}_1 + \mathbf{p}_2) \times (\rho_1 - \rho_2)]_z \end{aligned} \quad (35)$$

where the subscript z indicates the z -component of the vector product.

B. Darwin term

Let us now discuss the role of the Darwin terms, which also arise at linear order in the Berry curvature but as second derivatives of the interaction potential. The Darwin term of the j -th particle reads $|\Omega_j| \nabla^2 \hat{V}(\mathbf{r}_j)/4$, where the potential is again created by the remaining two particles, such that one obtains

$$\begin{aligned} H_D^T = & \frac{|\Omega_e(0)|}{4} \left[\nabla_{\mathbf{r}_1}^2 \hat{V}(\rho_1) + \nabla_{\mathbf{r}_h}^2 V(\rho_1) \right] \\ & + \frac{|\Omega_e(0)|}{4} \left[\nabla_{\mathbf{r}_2}^2 \hat{V}(\rho_2) + \nabla_{\mathbf{r}_h}^2 V(\rho_2) \right] \\ & - \frac{|\Omega_e(0)|}{4} \left[\nabla_{\mathbf{r}_1}^2 \hat{V}(|\rho_1 - \rho_2|) + \nabla_{\mathbf{r}_2}^2 \hat{V}(|\rho_1 - \rho_2|) \right] \end{aligned} \quad (36)$$

where we have again used $\Omega_e(\mathbf{p}) = -\Omega_h(\mathbf{p}) \simeq \Omega(0)/2$. Since $\nabla_{\mathbf{r}_1}^2 \hat{V}(\rho_1) = \nabla_{\mathbf{r}_h}^2 \hat{V}(\rho_1) = \nabla_{\rho_j}^2 \hat{V}(\rho_j)$ the Darwin

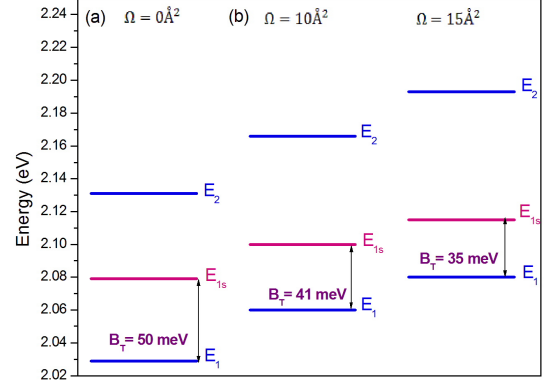


FIG. 2. Energies of low-lying trion states E_{1T} and E_{2T} , considering the ground exciton state E_{1s} . Calculations are performed on WS₂ monolayer using $\varepsilon_{sub} = 2.1$, $\lambda_s = 28\text{\AA}$, a) $\Omega = 0$, b) $\Omega = 10\text{\AA}^2$ and $\Omega = 20\text{\AA}^2$.

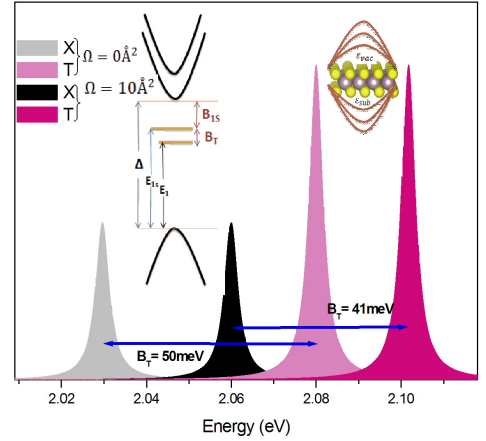


FIG. 3. Spectrum of a WS₂ monolayer showing the effect of Berry correction on exciton X and trion T energies. The parameters used are $\lambda_s = 28\text{\AA}$, $\varepsilon_{sub} = 2.1$ and $m_h = m_e = 0.34$.

term of the trion Hamiltonian reads [43]

$$\hat{H}_D^T = \frac{|\Omega(0)|}{4} \left[\nabla_{\rho_1}^2 \hat{V}(\rho_1) + \nabla_{\rho_2}^2 \hat{V}(\rho_2) - \nabla_{\rho_3}^2 \hat{V}(\rho_3) \right] \quad (37)$$

Collecting both the Berry-curvature correction and the Darwin term, the trion Hamiltonian is

$$\begin{aligned}
\hat{H}_T = & \frac{3\Delta}{2} + \frac{\mathbf{p}_1^2}{2\mu} + \hat{V}(\rho_1) \\
& + \frac{1}{2\hbar} \nabla_{\rho_1} \hat{V} \cdot [\Omega(0) \times \mathbf{p}_1] + \frac{|\Omega(0)|}{4} \nabla_{\rho_1}^2 \hat{V}(\rho_1) \\
& + \frac{\mathbf{p}_2^2}{2\mu} + \hat{V}(\rho_2) \\
& + \frac{1}{2\hbar} \nabla_{\rho_2} \hat{V} \cdot [\Omega(0) \times \mathbf{p}_2] + \frac{|\Omega(0)|}{4} \nabla_{\rho_2}^2 \hat{V}(\rho_2) \\
& + \frac{\mathbf{p}_1 \cdot \mathbf{p}_2}{2m_h} - \hat{V}(|\rho_1 - \rho_2|) \\
& - \frac{1}{2\hbar} \nabla_{\rho_3} \hat{V} \cdot [\Omega(0) \times (\mathbf{p}_1 + \mathbf{p}_2)] - \frac{|\Omega(0)|}{4} \nabla_{\rho_3}^2 \hat{V}(\rho_3)
\end{aligned} \tag{38}$$

This trion Hamiltonian can be easily expressed as a function of the exciton Hamiltonian (15)

$$\begin{aligned}
\hat{H}_T = & -\frac{\Delta}{2} + \sum_{i=1,2} \hat{H}_{X_i} + \frac{\mathbf{p}_1 \cdot \mathbf{p}_2}{2m_h} - \hat{V}(|\rho_1 - \rho_2|) \\
& - \frac{1}{2\hbar} \nabla_{\rho_3} \hat{V} \cdot [\Omega(0) \times (\mathbf{p}_1 + \mathbf{p}_2)] - \frac{|\Omega(0)|}{4} \nabla_{\rho_3}^2 \hat{V}(\rho_3)
\end{aligned} \tag{39}$$

As a first step towards solving the eigenvalue equation of the relative motion, we use a wave function expansion technique; it is factorized into

$$\begin{aligned}
\psi_T(\rho_1, \rho_2) = & \sum_{\tilde{n}, \tilde{m}} b_{\tilde{n}\tilde{m}} \frac{1}{\sqrt{2}} \{ \chi_{1\tilde{s}}(\rho_1) \chi_{\tilde{n}, \tilde{m}}(\rho_2) + \\
& \chi_{\tilde{n}, \tilde{m}}(\rho_1) \chi_{1\tilde{s}}(\rho_2) \},
\end{aligned} \tag{40}$$

where $\chi_{\tilde{n}, \tilde{m}} = \sum_{n, |m| < n} c_{nm} \varphi_{n, m}$ is the wave function solution of the exciton Hamiltonian, expanded in terms of 2D-hydrogenic state $\varphi_{n, m}(\rho, \theta)$. The number \tilde{n}, \tilde{m} refers to the dominant contribution of the coefficients c_{nm} to the excitonic function [28]. We emphasize that the trion wavefunction is a symmetric combination of only the $n\tilde{s}$ states. We denote the trion as symmetric in accordance with the symmetry of the wave function. According to Courtade et al. [44] the symmetric trion is stable within the effective mass approximation. Moreover, the trion wavefunction with symmetric combination is the ground state. Since, because we disregard the unstable antisymmetric trion, which can be represented by the antisymmetric combination of $m \neq 0$ states, hereafter the Berry correction is limited to the Darwin term contribution. To find the negative trion eigenvalues E_N , we have diagonalize a 5×5 Hamiltonian matrix. For a given in-plane trion center-of-mass wavevector $\mathbf{P}_T = 0$, we calculate in the following the trion binding energies for both WS₂ and WSe₂ monolayer.

C. Calculation of the trion binding energies

The trion binding energy B_T is conventionally introduced as the difference between the trion energy E_1 , i.e.,

the ground eigenenergy of the Hamiltonian (39), and the energy of the neutral exciton (15). In other words, the eigenvalue of the trion bound states is $E_1 = -(B_{1s} + B_T)$. Our study takes into account the strong dielectric contrast between the vacuum on top of the monolayer and the substrate below it, leading to a large trion binding energy close to that measured experimentally. We treat below λ_s and ε_{sub} as parameters of the theory, see Tab. III and Tab. IV (Tab. V) for discussion of particular values of WS₂ (WSe₂) monolayer. As predicted in Eq. (30), the resulting trion binding energy is a function of the screening length, the Berry curvature and probably the electron-hole mass ratio. For the WS₂ layer deposited on the top of the SiO₂ substrate ($\varepsilon_{sub} = 2.1$) and exposed to the air ($\varepsilon_{vac} = 1$), the energies of the first states of trions are plotted in Fig. 2. The screening length λ_s is fixed at 28Å, in the absence of the Darwin correction, the trion ground-state energy is $E_{1T} = 2.029$ eV and the first excited state is $E_{2T} = 2.131$ eV. In the trion spectrum, we show that the exciton energy E_{1s} (around 2.079 eV in this case) is always located far from E_{2T} . Therefore, we will focus only on the trion ground-state energy E_{1T} . By including the Berry correction, a blue-shift from the lowest trion energies is observed following the enhancement of the exciton energy. A monotone increasing of the energy states with Berry curvature is explained by the analytical form of Darwin term given by Eq. (37). The effective Darwin correction leads to an energy shift for all the states. The form of the lowest trion and exciton spectrum including the Berry curvature correction is shown in Fig. 3. The trion binding energy B_T is calculated for the same parameters as those used in Fig. 2. The state X represents the neutral 1s exciton and the corresponding negatively charged trion labeled as T. This plot shows the decrease of B_T by including the Darwin term as well as, the decrease of B_{1s} by about 22 meV. The results are in line with our findings for the neutral excitons, where the inclusion of the Darwin term correction reduces the binding energy. Indeed, in the presence (absence) of Berry curvature effects, particularly the Darwin term we obtain 288 meV (310 meV) for the exciton binding energy and 41 meV (50 meV) for that of the trion. The parameters used are: $\lambda_s = 28$ Å, $\varepsilon_{sub} = 2.1$, $m_e = m_h = 0.34$ and $\Omega = 10$ Å². This result converges towards the experimental data given by Molas *et al.* [50].

Clearly, the trion binding energies show a large dependence on the Berry curvature, varying by 8 meV or more, in agreement with the experiment using SiO₂ as a substrate [51]. This trend is generic, as one can see from Tab. III, where we have given the trion binding energy for various values of the screening length λ_s . In comparison with experimental measurements, our results suggest that the screening length may be around 5.5 a_B and 6.5 a_B for both WS₂ and WSe₂ monolayer. It is important to notice that the main difference between WS₂ and WSe₂ monolayer resides only on the effective mass of the charge carriers.

Let us now briefly discuss the role of dielectric envi-

TABLE III. Trion binding energies (given in meV) for both WS₂ and WSe₂ monolayer. Experimental and theoretical results from literature are collected for comparison. The reduced mass used are listed in Ref. [28, 45] and $\epsilon_{sub} = 2.1$, corresponding to an effective Bohr radius of $\sim 5\text{\AA}$.

$\lambda_s (a_B)$	$\Omega = 0$		$\Omega = 10 \text{\AA}^2$	
	WS ₂	WSe ₂	WS ₂	WSe ₂
4.5	67	61	59	54
5.0	61	56	53	49
5.5	55	51	46	44
6.0	49	47	41	40
6.5	43	41	35	34
system	WS ₂		WSe ₂	
Experiment	34 [46]-36[13]-45[47]-47[48]		30[35]-35[44]-47[48]	
Theory	31[49]-34[37]		26[44]-27[49]-30[37]	

TABLE IV. Exciton and trion binding energies for monolayer WS₂ exposed to the air and deposited in different substrates described by ϵ_{sub} and for a range of screening lengths λ_s .

$\epsilon_{sub}(\epsilon_0)$	$\kappa(\epsilon_0)$	$\Omega (\text{\AA}^2)$	$\lambda_s = 20\text{\AA}$		$\lambda_s = 25\text{\AA}$		$\lambda_s = 30\text{\AA}$	
			$B_{1s}(\text{meV})$	$B_T(\text{meV})$	$B_{1s}(\text{meV})$	$B_T(\text{meV})$	$B_{1s}(\text{meV})$	$B_T(\text{meV})$
1.5	1.25	0	510	88	449	67	402	48
		10	457	70	409	49	371	36
2.1	1.55	0	372	72	330	56	297	44
		10	338	61	305	46	278	35
2.5	1.75	0	311	62	277	52	250	41
		10	284	55	257	45	235	34

ronment described by the effective dielectric constant κ on the trion and exciton binding energies. By taking into account the Berry curvature correction, Tab. IV (Tab. V) shows different values for the binding energies in WS₂ (WSe₂) upon variation of the average dielectric constant of the surrounding material and screening length. When the screening length vanishes which corresponds to the strictly 2D limit of a Coulomb problem, the exciton binding energy is ~ 4 Ry and the trion binding energy reaches its maximum values. With increasing λ_s , the Coulomb potential becomes shallow and both the exciton and trion binding energies decrease. On the other hand, the calculated trion and exciton binding energies of a monolayer encapsulated between two layers of varying dielectric constants increase upon decrease of the effective dielectric constant κ . This behavior is explained by the fact that the exciton binding energy scales as $\sim 1/(\lambda_s \kappa)$. The Darwin term correction lowers the relatively large trion binding energy inherited from neutral exciton [22]. The Berry curvature Ω has a similar effect in the trion binding energy, i.e. it decreases with increasing Berry curvature, similarly to the binding energy of the neutral exciton. For $\lambda_s = 30\text{\AA}$, $\Omega = 10\text{\AA}^2$ and $\kappa = 1.55$ corresponding to a SiO₂ substrate, the trion binding energy of WS₂ monolayer is around 35 meV, which is in excellent agreement with the value of 34 meV reported in Ref. [46]. Accordingly, the exciton binding energy is around 278 meV, using the same λ_s , which is somewhat lower than exper-

imental values of 340 meV. In order to reproduce the experimental exciton and trion binding energies of about 300 and 42 meV at 7K, respectively [52], we use $\lambda_s = 28\text{\AA}$ for a WS₂ monolayer on SiO₂ substrate. In similar structures but made of WSe₂ monolayer, $B_{1s} = 290$ meV for a sample placed on SiO₂ substrate $\epsilon_{sub} = 2.1$ which is in agreement with reported in Ref. [53] using $\lambda_s = 26\text{\AA}$. A relatively small exciton binding energy around 160 meV has been extracted for a WSe₂ monolayer encapsulated in hBN [12]. As one expects, the increase of the dielectric constant lowers the characteristic energies, while keeping the binding energy lower if the Berry curvature is taken into account as compared to $\Omega = 0$. It should be noted that our calculation concern only the intra-valley trion which involves a pair of electrons from the same subband in the conduction band.

IV. DISCUSSION AND CONCLUSIONS

In conclusion, we have investigated the role of Berry-curvature corrections in the energies of symmetric intravalley charged excitons (trions). The analysis is based on previous work on neutral excitons [20–22], which we have reviewed in the first part of our paper.

With this modified Hamiltonian, the Berry curvature changes the neutral and charged exciton binding energy, mixing and splitting angular momentum states and reor-

TABLE V. Exciton and trion binding energies for monolayer WSe₂ exposed to the air and deposited in different substrates described by ε_{sub} and for a range of screening lengths λ_s .

		$\lambda_s = 20\text{\AA}$		$\lambda_s = 25\text{\AA}$		$\lambda_s = 30\text{\AA}$		
$\varepsilon_{sub}(\varepsilon_0)$	$\kappa(\varepsilon_0)$	$\Omega (\text{\AA}^2)$	$B_{1s}(\text{meV})$	$B_T(\text{meV})$	$B_{1s}(\text{meV})$	$B_T(\text{meV})$	$B_{1s}(\text{meV})$	$B_T(\text{meV})$
1.5	1.25	0	491	86	433	69	389	52
		10	442	74	397	58	361	42
2.1	1.55	0	357	67	318	57	287	47
		10	326	60	295	50	269	40
4	2.5	0	171	26.9	155	25.7	142	24.5
		10	160	26	147	25	136	23.9

ganizing the spectrum. The result is that the different angular momentum states for each energy level n have their energies split from each other. On the other hand, the Darwin term leads to an energy shift depending on the radial quantum number n . Furthermore, the charged trion energy is also found to exhibit a strong shift since it depends on exciton states, as anticipated in Eq (30). Tables IV and V contain our complete findings for the exciton and trion binding energies dependence on the Berry curvature for a range of screening lengths and relative dielectric constants of the bottom substrate. First, the decrease of the exciton and trion binding energies is due to the strong dielectric screening by the surrounding environment even for $\Omega \neq 0$. Second, in addition to the effect of the dielectric environment surrounding the sample, the behavior of the binding energies is also related to changes in the Berry curvature. For the same substrate (i.e. for fixed ε_{sub}) and by varying the screening length, the Berry correction acts dramatically for a relatively

large exciton binding energy corresponding to small λ_s . Consequently, the trion binding energy shifted by about 20 meV and sometimes exceeds the experimental findings. This may explain the significant TMDs monolayer exciton and trion binding energies discrepancy using for example SiO₂ substrate, i.e. $\varepsilon_{sub}=2.1$, and thus $\kappa = 1.55$. Berry-curvature effects are less important for relatively weak exciton and trion binding energy. Our results exhibit relatively agreement with those of Ref. [52]. Similar to the findings for exciton binding energy by varying λ_s or ε_{sub} , the trion binding energy reacts most sensitively to changes in Ω . The most striking feature of the trion binding energy dependence on Berry correction is $B_T(\Omega) - B_T(0) = [B_X(\Omega) - B_X(0)]/2$

Finally, by examining the excitonic spectrum, we have shown that the degeneracy of 2D excitonic states is lifted due to the inclusion of the Berry curvature. The result is a dramatic reorganization of the excitonic spectrum, producing thus a new distribution of trion states.

-
- [1] D. Xiao, G-B. Liu, W. Feng, X. Xu, and W. Yao, Phys. Rev. Lett. **108**, 196802 (2012).
- [2] A. M. Jones, H. Yu, N. J. Ghimire, S. Wu, G. Aivazian, J.S. Ross, B. Zhao, J. Yan, D. G. Mandrus, D. Xiao, W. Yao, X. Xu, Nat. Nanotech. **8**, 634 (2013).
- [3] G-B Liu, W-Y Shan, Y. Yao, W. Yao, and D. Xiao, Phys. Rev. B **88**, 085433 (2014).
- [4] X. Xu, W. Yao, D. Xiao and T. F. Heinz, Nat. Phys. **10**, 343 (2014).
- [5] H. Yu, G. Liu, P. Gong, X. Xu and W. Yao Nat. Commun. **5**, 3876 (2014).
- [6] M. M. Glazov, T. Amand, X. Marie, D. Lagarde, L. Bouet, and B. Urbaszek, Phys. Rev. B **89**, 201302(R) (2014).
- [7] F. Wu, F. Qu, and A. H. MacDonald, Phys. Rev B **91**, 075310 (2015).
- [8] J. R. Schaibley, H. Yu, G. Clark, P. Rivera, J. S. Ross, K. L. Seyler, W. Yao and X. Xu, Nat. Rev. Mats. **1**, 55 (2016).
- [9] A. V. Stier, N. P. Wilson, G. Clark, X. Xu, and S. A. Crooker, Nano Lett. **16**, 7054 (2016).
- [10] S. Borghardt, J-S Tu, F. Winkler, J. Schubert, W. Zander, K. Lesson, B. E. Kardyna, Phys. Rev. Mats. **1**, 054001 (2017).
- [11] G. Wang, A. Chernikov, M. M. Glazov, T. F. Heinz, X. Marie, T. Amand, B. Urbaszek, Rev. Mod. Phys. **90**, 21001 (2018).
- [12] D. Vaclavkova, J. Wyzula, K. Nogajewski, M. Bartos, A. O. Slobodeniuk, C. Faugeras, M. Potemski, M. R. Molas, Nanotechnology, **29**, 32 (2018).
- [13] A. Chernikov, T. C. Berkelbach, H. M. Hill, A. Rigosi, Y. Li, O. B. Aslan, D. R. Reichman, M. S. Hybertsen, and T. F. Heinz, Phys. Rev. Lett. **113**, 076802 (2014).
- [14] K. He, N. Kumar, L. Zhao, Z. Wang, K. F. Mak, H. Zhao, and J. Shan, Phys. Rev. Lett. **113**, 026803 (2014).
- [15] A. T. Hanbicki, M. Currie, G. Kioseoglou, A. L. Friedman, and B. T. Jonker, Solid State Commun. **203**, 16 (2015).
- [16] G. Gupta, S. Kallatt, and K. Majumdar, Phys. Rev. B **96**, 081403(R) (2017).
- [17] Z. Ye, T. Cao, K. OBrien, H. Zhu, X. Yin, Y. Wang, S.G. Louie, and X. Zhang, Nature **513**, 214 (2014).
- [18] Y. Lin, X. Ling, L. Yu, S. Huang, A. L. Hsu, Y-H. Lee, J. Kong, M. S. Dresselhaus, and T. Palacios, Nano Lett. **14**, 5569 (2014).
- [19] A. V. Stier, K. M. McCreary, B. T. Jonker, J. Kono and

- S. A. Crooker, Nat Commun. **7**, 10643 (2016).
- [20] J. Zhou, W-Y Shan, W. Yao, and D. Xiao, Phys. Rev. Lett. **115**, 166803 (2015).
- [21] A. Srivastava and A. Imamoglu Phys. Rev. Lett. **115**, 166802 (2015).
- [22] M. Trushin, M. O. Goerbig, and W. Belzig, Phys. Rev. Lett. **120**, 187401 (2018).
- [23] D. Xiao, M.-C. Chang, and Q. Niu, Rev. Mod. Phys. **82**, 1959 (2010).
- [24] This can be achieved if we substitute $\partial\hat{H}_0/\partial\mathbf{\Pi} \simeq \dot{\mathbf{R}}$ and $\partial\hat{V}/\partial\mathbf{R} \simeq -\dot{\mathbf{\Pi}}$, in the corresponding equations, the corrective terms being of higher order in B and Ω_α .
- [25] W. Yao and Q. Niu, Phys. Rev. Lett. **101**, 106401 (2008).
- [26] I. Garate and M. Franz, Phys. Rev. B **84**, 045403 (2011).
- [27] M. Trushin, M. O. Goerbig, and W. Belzig, Phys. Rev. B **94**, 041301(R) (2016).
- [28] A. Hichri, I. Ben Amara, S. Ayari, and S. Jaziri, J. Appl. Phys. **121**, 235702 (2017); A. Hichri, I. Ben Amara, S. Ayari and S. Jaziri ; J. Phys.:Cond. Matt. **29**, 435305 (2017).
- [29] Notice that the maximal value of the Berry curvature $\Omega = \hbar^2/\mu\Delta$ is obtained in the model of massive Dirac fermions, with only the gap Δ in the diagonal matrix elements of the 2D Dirac Hamiltonian. If these elements are modified by a parabolic correction, the mass term is generically enhanced and the Berry curvature decreases, see: M. O. Goerbig, G. Montambaux, and F. Piéchon, Europhys. Lett. **105**, 57007 (2014).
- [30] L. V. Keldysh, JETP Lett. **29**, 658 (1979).
- [31] P. Cudazzo, I. V. Tokatly, and A. Rubio, Phys. Rev. B, **84**, 085406 (2011).
- [32] G. Berghuser A. Knorr, and E. Malic, 2D Mater **4** 015029 (2017).
- [33] J. Xiao, M. Zhao, Y. Wang, and X. Zhang Nanophotonics **6**, 1309 (2017).
- [34] Dinh Van Tuan,1 Min Yang,1 and Hanan Dery,arxiv.org/abs/1801.00477v1.
- [35] G.Wang X. Marie, I. Gerber, T. Amand, D. Lagarde, L. Bouet, M. Vidal, A. Balocchi and B. Urbaszek,Phys. Rev. Lett. **114**, 097403 (2015).
- [36] I. Klyachko and H.-P. Komsa, Phys. Rev. B **92**, 205418 (2015).
- [37] David K. Zhang, Daniel W. Kidd, and Kaálmaán Varga, acs.nanolett.5b03009 (2015).
- [38] A. Ramasubramanian, Phys. Rev. B **86**, 115409 (2012).
- [39] A. Singh, G. Moody, K. Tran, M. E. Scott, V. Overbeck, G. Berghuser, J. Schaibley, E. J. Seifert, D. Pleskot, N. M. Gabor, J. Yan, D. G. Mandrus, M. Richter, E. Malic, X. Xu, and X. Li, Phys. Rev. B **93**, 41401 (2016).
- [40] B. Stébé et al., Phys. Rev. B **56**, 12454 (1997); A. Esser, E. Runge, and R Zimmermann, Phys. Rev. B **62** 8232 (2000); T. C. Berkelbach, M. S. Hybertsen, and D. R. Reichman, Phys. Rev. B **88**, 045318 (2013).
- [41] Notice, however, that it is strictly speaking a redundant variable that can be expressed in terms of ρ_1 and ρ_2 .
- [42] Corrections beyond this approximation are parabolic in the wave vector and would thus lead to terms of order $\vartheta(p^3)$ in HB that are also neglected in the kinetic term of the band Hamiltonian.
- [43] Notice that the validity of this result does not depend on the assumption $\Omega_e(p) = -\Omega_h(p)$, which is only valid in a true two-band model. In this case, one needs to simply consider the exciton Berry curvature as the difference between the two, $\Omega(0) = \Omega_e(0) - \Omega_h(0)$.
- [44] E. Courtade, M. Semina, M. Manca, M. M. Glazov, C. Robert, F. Cadiz, G. Wang, T. Taniguchi, K. Watanabe, M. Pierre, W. Escoffier, E. L. Ivchenko, P. Renucci, X. Marie, T. Amand, and B. Urbaszek, Phys. Rev. B **96**, 085302 (2017).
- [45] F. A. Rasmussen and K. S. Thygesen, J. Phys. Chem. C **119**, 13169 (2015).
- [46] B. Zhu, X. Chen, and X. Cui, Sci. Rep. **5**, 9218 (2015).
- [47] B. Zhu, H. Zeng, J. Dai, Z. Gong, X. Cui, Proc. Natl. Acad. Sci. USA. **111**, 11606 (2014).
- [48] M R Molas, C Faugeras, A O Slobodeniuk, K Nogajewski, M Bartos, D M Basko and M Potemski, 2D Mater. **4**, 021003 (2017).
- [49] M. Szytniszewski, E. Mostaani, N. D. Drummond, and V. I. Falko, Phys. Rev. B **95**, 081301(R) (2017).
- [50] Maciej . Molas, Karol Nogajewski, Artur Slobodeniuk, Johannes Binder, Miroslav Bartos, and Marek Potemski, Nanoscale **9**, 13128 (2017)
- [51] G. Plechinger, P. Nagler, J. Kraus, N. Paradiso, C. Strunk, C. Schüller, and T. Korn, Phys. Status Solidi RRL **9**, 457 (2015).
- [52] J Jadczyk, J Kutrowska-Girzycka, P Kapucinski, Y S Huang, A Wajs and L Bryja, Nanotechnology **28**, 395702 (2017).
- [53] A. Raja, A. Chaves, J. Yu, G. Arefe, H. M. Hill, A. F. Rigosi, T. C. Berkelbach, Ph. Nagler, C. Schuller, T. Korn, C. Nuckolls, J. Hone, L. E. Brus, T. F. Heinz, D. R. Reichman and A. Chernikov, Nat Commun. **8**, 15251 (2017).